Shape Changes of C_{16}TABr Micelles on Benzene Solubilization

Niklas Hedin,[†] Ruslan Sitnikov,[†] István Furó,*[,†] Ulf Henriksson,[†] and Oren Regev[‡]

Division of Physical Chemistry, Department of Chemistry, Royal Institute of Technology, SE-100 44 Stockholm, Sweden, and Department of Chemical Engineering, Ben-Gurion University of the Negev, Box 653, IL-84105 Beer-Sheva, Israel

Received: May 24, 1999; In Final Form: September 3, 1999

The microstructure of C_{16}TABr micelles with solubilized benzene was investigated by field-dependent ^{2}H NMR spin relaxation of C_{16}TABr-α-d_2. The relaxation data, supported by cryogenic transmission electron microscopy that excludes oblate micelle shapes, suggest that the C_{16}TABr micelles, slightly elongated even without benzene, become longer and more polydisperse on benzene addition. Field-dependent ^{2}H spin relaxation measurements on the benzene (C_6D_6) indicate that at low solubilizate content the benzene is predominantly located at the micellar interface, reorients more slowly than in bulk, and has a high lateral diffusion coefficient. Above a particular benzene concentration, the surfactant relaxation data suggest no further elongation but a radial growth, while the benzene relaxation shows that a large part of the benzene is residing in an interior region with near-bulk characteristics; the micelles become slightly elongated microemulsion droplets.

Introduction

As has been firmly established by a stream of recent studies, solubilizing small molecules in micelles often leads to changes in the aggregate structure.[1−3] This structural transformation, caused by rather small shifts within the balance upheld among the various strong molecular interactions within and around the aggregate, is far from being completely understood. As one curious example, addition of cyclic and linear aliphatic hydrocarbons to hexadecyltrimethylammonium bromide (C_{16}TABr) micelles induces different sequences of structural changes.[3] Since both of these molecule types preferentially reside in the micellar interior, the displayed divergence may appear through their differing influence on the chain packing. In contrast, aromatic hydrocarbons and alcohols are widely believed to prefer the headgroup region of cationic micelles[1,2,4−8] and therefore may primarily modify the headgroup−headgroup interactions. To widen our scope in this direction, the present work investigates the solubilizate-induced structural changes on addition of benzene to C_{16}TABr micelles.

At the outset, we have the following prior information. First, static viscosity[4,9] shows an initial increase up to a maximum and then a decrease when even more benzene is added. (No similar increase of viscosity is detected in C_{16}TACl solutions.[9]) Second, ^{1}H NMR presents larger chemical shift changes on benzene addition for methylene protons closer to the headgroup than that for the ones further away from the headgroup.[4,5] Short of a proof,[10] this effect is nevertheless an indication of preferential location of the benzene in the headgroup region. As an additional support, benzene has a higher molecular order parameter than cyclohexane in the hexagonal C_{16}TABr−solubilizate−water phase.[7,8]

Information on micellar structure can be obtained by several methods, two of which, field-dependent ^{2}H NMR spin relaxation and cryogenic transmission electron microscopy (cryo-TEM), are employed in this work. Choosing ^{2}H NMR facilitates comparing our findings to previous ones from the same laboratory and to ones on related systems. Moreover, as shown below, this method will provide us with parallel information on the molecular dynamics of both the benzene and the surfactant molecules, which lends some internal consistency to our interpretation of the experimental data.

Experimental Section

Hexadecyltrimethylammonium bromide deuterated in the α-position (C_{16}TABr-α-d_2) was synthesized as described elsewhere.[11] A 3.6 wt % (0.10 mol/kg H_2O) stock solution of C_{16}TABr-α-d_2 was prepared with deuterium-depleted water (Isotec). This solution filled short (4−5 cm) NMR tubes up to a level of ∼3 cm. After benzene was added, the tubes were flame-sealed. Closed short tubes were chosen to minimize the evaporation of the benzene from the micellar phase that may thereafter be condensed on the top of the tube. The amount of the added benzene, given below as the mole ratio X = (mole benzene)/(mole surfactant), was determined from the integral intensities of the benzene and surfactant ^{1}H NMR lines. (The solubility of benzene in water is 2 orders of magnitude lower than our benzene concentrations in the investigated micellar phase.[12]) In samples containing perdeuterated benzene C_6D_6, the benzene content was established via ^{2}H NMR integral intensities; at high fields (≥4.7 T) the two ^{2}H NMR signals from C_6D_6 and C_{16}TABr-α-d_2 are well separated. Note that the ^{2}H spin relaxation of C_6D_6 was only measured at such high fields.

^{2}H NMR. Field-dependent ^{2}H NMR spin relaxation measurements were performed at 30 °C, safely above the Krafft point of neat C_{16}TABr solutions,[13−15] on a Bruker MSL 90/200 spectrometer equipped with an electromagnet (2−13 MHz for ^{2}H) and a cryomagnet (30.7 MHz) and on Bruker AMX300 (46.1 MHz) and Bruker DMX500 (76.8 MHz) spectrometers. The longitudinal relaxation rate $R_1 = 1/T_1$, where T_1 is the corresponding relaxation time, was measured in a conventional inversion recovery experiment with an extended phase cycle

* To whom correspondence should be addressed. Phone: +46 8 790 8592. Fax: +46 8 790 8207. E-mail: ifuro@physchem.kth.se.
† Royal Institute of Technology.
‡ Ben-Gurion University of the Negev.

10.1021/jp991686o CCC: $18.00 © 1999 American Chemical Society
Published on Web 10/16/1999

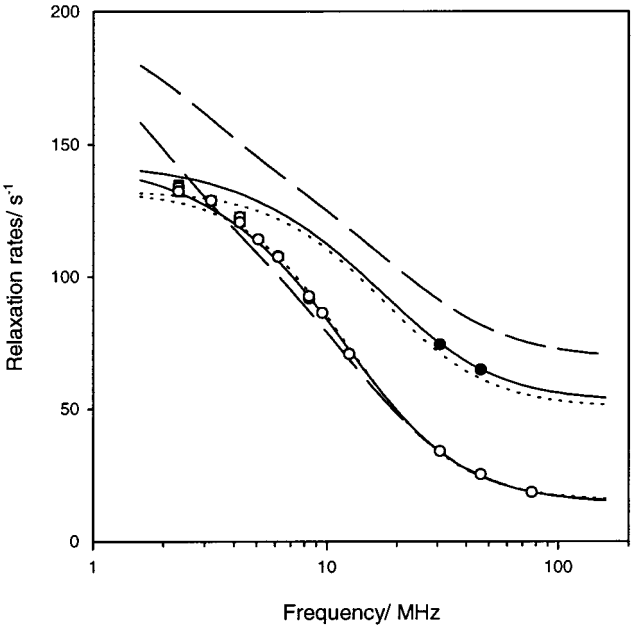

Figure 1. Frequency dependence of the ^{2}H relaxation rates of C_{16}TABr-α-d_2 in a 0.10 *m* C_{16}TABr solution. Empty and full symbols refer to the longitudinal (R_1) and transverse (R_2) relaxation rates, respectively. The theoretical expressions for prolate micelles with fixed axial ratios $\rho = 1.0$ (dotted line), $\rho = 1.6$ (solid line), and $\rho = 2.2$ (dashed line) have been fitted to the experimental data.

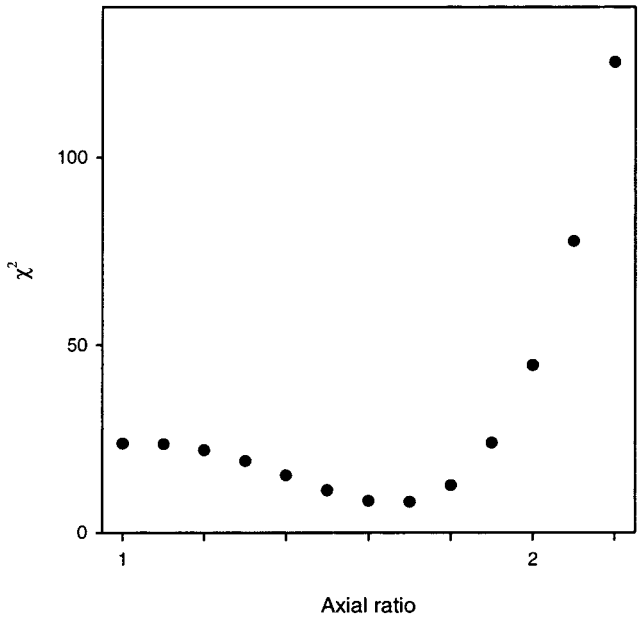

Figure 2. Reduced χ^2 merit function (χ in this expression is not connected to the quadrupole coupling constant (see eqs 1 and 2), which is conventionally denoted by the same Greek character) plotted as the function of the axial ratio ρ (set as a fixed fitting parameter). χ^2 is the sum of the squares of the deviations between the experimental and theoretical relaxation rates, divided by the estimated individual experimental error estimate squares (see Experimental Section) and by $N =$ (the number of data points) − (the number of free parameters).

and with a recycle delay of $>5T_1$. The transverse relaxation rate R_2 was measured by the spin echo sequence with Exorcycle;[16] choosing this pulse sequence instead of a CPMG pulse train increases the experimental time (to achieve the same level of random error) but makes it easier to quantify the actual experimental error of the relaxation rates.

As an essential point, both experiments used a random variation of the delay times within the applied pulse sequences. This arrangement renders all errors, caused by slow instrumental drifts (temperature, field, signal intensity, pulse power) during the actual experiment, to be well estimated by the error obtained as the average least-squares deviation of the experimental points from the fitted exponential curves. This error increases with the length of the experiment and is one of the two major components of the total error presented in Figures 1 and 3−5. To reduce it, the field stability of the electromagnet system has been improved.[17] The other major component of the full errors presented in the figures is the set-temperature uncertainty. To achieve a reproducible temperature, the actual temperature was established from the temperature-sensitive ^{59}Co chemical shift of $CoK_3(CN)_6$ dissolved in water[18] (as shift reference we used the ^{23}Na signal of NaCl dissolved in the same solution); this arrangement provided us with a maximal set-point error of ±0.05 K. The temperature sensitivity of the relaxation rates has also been established (most sensitive are the transverse relaxation rates, with about 1%/0.2 K variation). All contributions collected, the largest estimated total errors ($\pm 1\sigma$) of the relaxation rates, were those of the lowest-frequency R_1 points: (±1.5%) − (±2.2%) for the different samples. The other points have errors about or less than ±1%, and the error bars are smaller than the symbols representing the relaxation rates in Figures 1 and 3−5. Note that in Figure 1 the presented data points are from two separate experiments; in those two experiments such as in other tests (not shown) the reproducibility of the obtained relaxation rates was within the random errors specified above.

Cryo-TEM. The vitrified specimens for cryo-TEM[19] were prepared in a controlled environment vitrification chamber[20] at room temperature with the relative humidity kept close to 100%. A 5 μL drop of the surfactant solution was put on a TEM grid supported by carbon-coated perforated polymer film that was then gently blotted by filter paper, creating a thin film of the liquid over the grid. Immediately after the blotting, the grid was rapidly plunged into liquid ethane and then transferred under a liquid nitrogen environment to a cold stage (Gatan 626) and into the electron microscope (JEOL 1200EXII), operated at 100 kV in conventional TEM mode.

^{2}H Spin Relaxation in Micellar Aggregates

The relaxation of ^{2}H is dominated by its randomly fluctuating quadrupole interaction. The quadrupolar spin relaxation of an $I = 1$ spin in a macroscopically isotropic (i.e., without a static quadrupole coupling) solution can be expressed with the help of the reduced motional spectral densities $j(\omega)$ of the spin-bearing nuclei as[21]

$$R_1 = T_1^{-1} = \frac{3\pi^2\chi^2}{40}(2j(\omega_0) + 8j(2\omega_0)) \quad (1)$$

$$R_2 = T_2^{-1} = \frac{3\pi^2\chi^2}{40}(3j(0) + 5j(\omega_0) + 2j(2\omega_0)) \quad (2)$$

In these expressions, χ is the quadrupole coupling constant (qcc) experienced by the nuclear spin in the particular molecule while ω_0 is the Larmor frequency (rad s^{-1}) at the applied magnetic field. The accurate values of χ are somewhat controversial, but no major conclusion of this paper is affected by slight deviations from our choice of 167 kHz[22] for χ in C_{16}TABr-α-d_2 and 187 kHz[23] for χ in C_6D_6. If molecular motions of the probe nucleus, which average out the nuclear quadrupole interaction to zero, proceed on the $1/\omega_0$ time scale, the spectral densities $j(\omega)$ involved in the relaxation rates are frequency-dependent, which leads to frequency-dependent relaxation rates as well. In short,

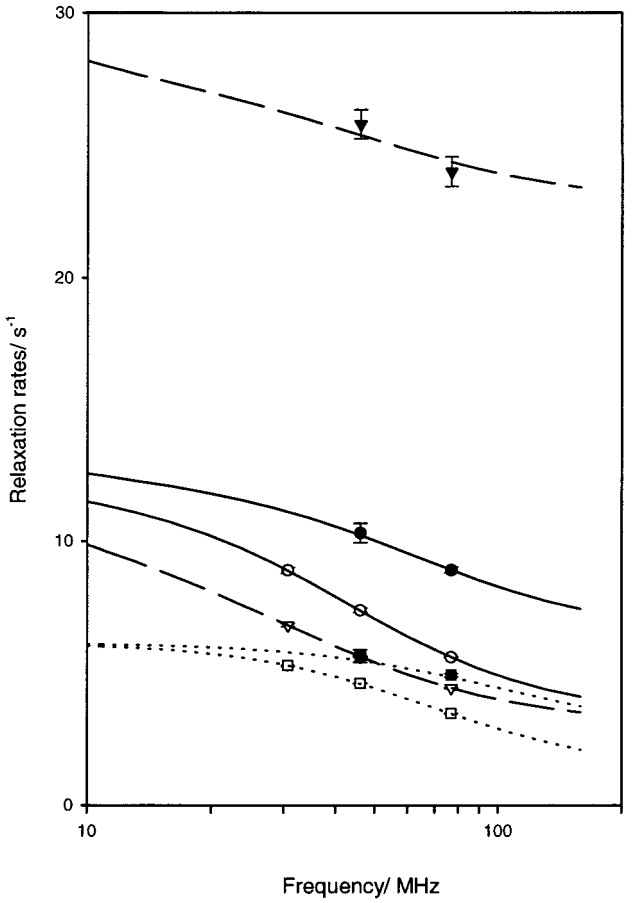

Figure 3. Frequency dependence of the ^2H relaxation rates R_1 (empty symbols) and R_2 (full symbols) of C_6D_6 solubilized in a 0.10 *m* $C_{16}TABr$ solution. The corresponding theoretical fits (see text) are presented as solid ($X = 0.3$; ○), dashed ($X = 1.0$; ▽), and dotted ($X = 2.0$; □) lines, with the obtained parameters in Tables 2 and 3.

we obtain nuclear magnetic relaxation dispersion (NMRD). Conversely, NMRDs (such as the ones presented in Figures 1 and 3−5) can be used for studying the underlying molecular dynamics.[3,11,24−27] The frequency window, defined by the accessible NMR frequencies, determines the time scale of motions to which the data are sensitive. Fortunately, micellar tumbling and the diffusion of the molecular components within the micelles fall close to or within the time scale provided by conventional NMR spectrometers and can hence be studied via NMRD.

For a surfactant molecule in a micelle, motions fast on the <0.1 ns time scale (such as chain isomerization) do not contribute to the NMRD and only provide a frequency-independent contribution to the spin relaxation. On the other hand, they partially average the quadrupole coupling to a residual value, which is further modulated by slower molecular motions. This residual quadrupole coupling is not zero, since the fast molecular motions of a surfactant molecule within an aggregate are anisotropic because of the presence of the hydrocarbon−water interface. This effective time scale separation is expressed as[28−30]

$$j(\omega) = S_{CD}^2\, j_s(\omega) + j_f \tag{3}$$

where S_{CD}, for ^2H spins in a methylene group, is the generalized order parameter of the C−D bond relative to the normal to the aggregate surface. NMR is not particularly sensitive to the details of the involved fast motions; j_f solely depends on the integral of the initial (<0.1 ns) decay of the time correlation function of the quadrupole interaction. Usually, this is expressed by a single effective correlation time τ_f as

$$j_f = 2(1 - S_{CD}^2)\tau_f \tag{4}$$

In isotropic micellar systems, the residual quadrupole coupling, its direction defined at a particular point by the water−hydrocarbon interface normal, is averaged to zero by the lateral surface diffusion of the surfactants and by the tumbling of the whole aggregate, both motions of which modulate the direction of the interface normal with respect to the applied magnetic field. For spherical aggregates these processes yield a convenient analytical expression for $j_s(\omega)$. For anisomeric micelles, one must instead rely on numerical solutions available in particular model geometries; in this paper, we apply the results of Halle[31] for uniaxial ellipsoids. There, micellar tumbling is treated as free Brownian motion of a rigid and smooth symmetric top. Moreover, the surface of the symmetric top is assumed to define the surface on which the diffusion of the surfactant molecules can be represented as free (i.e., where the diffusion equation is force-free, leading to a Gaussian spatial propagator). The surface diffusion and the micellar tumbling are statistically independent, and the resulting spectral density $j_s(\omega)$ is determined by the size and shape of the micelles and the lateral diffusion coefficient D_{lat} of the surfactant via the rotational correlation times τ_m^{rot} ($m = 0, 1, 2$) of the micelle and a characteristic diffusion time τ_{diff} of the surfactant molecule:

$$j_s(\omega) = j_s(\omega;\tau_{diff},\tau_m^{rot}) \tag{5}$$

The rotational correlation times τ_m^{rot} can be calculated as functions of the minor semiaxis r and the axial ratio ρ from the Perrin equations for a given viscosity of the surrounding medium, and the diffusion time τ_{diff} is given by

$$\tau_{diff} = \frac{r_{diff}^2}{D_{lat}} \tag{6}$$

The surface diffusion of a surfactant molecule is determined by its intermolecular interactions. Since the measured D_{lat} is very low compared to the diffusion coefficients of hydrocarbons of equal length in bulk, one can plausibly assume that the dominating interactions are the headgroup−headgroup ones. Thus, r_{diff} is defined by the maximum of the headgroup charge density. Because the α-d_2 segment is covalently connected to the headgroup, the *angular* correlation functions describing the modulation of the residual quadrupole coupling by surface diffusion are the same as the *angular* correlation functions for the headgroup motion. Equation 5 involves these angular correlation functions.

On the other hand, micellar tumbling is defined by the "hydrodynamic" extent of the aggregate, r_{hydro}; in a surfactant aggregate this particular measure can be approximated by the radius of the hydrocarbon interior plus the full headgroup diameter. The complication caused by this difference of the two involved radii is easy to handle, since the spectral density in eq 5 does not directly depend on r_{diff} but rather on the characteristic diffusion time τ_{diff} defined by eq 6. Hence, fitting our theoretical expressions to the experimental data can be performed by (i) setting the micellar radius to an assumed r_{hydro}, which then accounts for the micellar tumbling and then by (ii) obtaining τ_{diff} from the actual fitting. D_{lat} can then be calculated with the help of eq 6. Calculated in this way, the lateral diffusion

coefficient falls close to the value measured, e.g., by PGSE NMR in liquid crystalline phases.[32] The evaluation of the experimental data below is performed under the explicit assumption that

$$r_{\mathrm{diff}} = r_{\mathrm{hydro}} - d_{\mathrm{methyl}} \tag{7}$$

where the "diameter" of the methyl group d_{methyl} is set to 2.3 Å.

As shown below, evidence from scattering and cryo-TEM measurements favors prolates to oblates for the micellar shape. Because, as for C_{16}TABr micelles without solubilizate and with solubilized alkanes, monodisperse prolates do not suffice to credibly describe all our experimental data, we must introduce polydispersity in our model. Since surfactant molecules exchange rapidly among various aggregates on the time scale of the spin relaxation times, the obtained relaxation rates become simple molecular population averages,

$$j_{\mathrm{s}}(\omega) = \int_1^\infty j_{\mathrm{s}}(\omega;\rho)\, p(\rho)\, \mathrm{d}\rho \tag{8}$$

In this expression, $p(\rho)$ is the probability of finding a molecule in an aggregate of axial ratio ρ. τ_{f} and S_{CD} are assumed to be insensitive to micellar shape. Theoretical models for the polydispersity of micellar aggregates often yield a distribution function[33,34]

$$p(\rho) \propto \rho\, \mathrm{e}^{-\rho/\rho_0} \tag{9}$$

which we, with proper normalization, select as our model of polydispersity. The sharp lower limit, at $\rho = 1$, corresponds to spherical micelles with a fixed radius. In this particular model of polydispersity, the (molecular) average value of the axial ratio $\langle\rho\rangle$ is $2\rho_0 + (1 + \rho_0)^{-1}$, where ρ_0 is defined in eq 9. The distribution $p(\rho)$ according to eq 9 is based on the calculation of the entropy of mixing as in ideal solutions, i.e., using the mole fractions of the micelles with different sizes. Calculating ΔS_{mix} using volume fractions[35,36] instead gives a distribution $p(\rho)$ without the preexponential factor in eq 9. However, our experience with different distribution functions showed that the average axial ratio is rather insensitive to this choice; the obtained average axial ratios do not differ more than 10−20%.

The chosen representation of polydispersity, eq 9 or others of similar type, is attractive, since polydispersity is included without introducing additional model parameters. The price is that the average size and the polydispersity are not independent from each other. More sophisticated models could, in principle, be applied, but NMRD data usually do not suffice to determine the extra parameters associated with those size distributions.

Results and Discussion

Neat C_{16}TABr Micelles. Already at the very beginning of structural studies of surfactant aggregates, one suspected the existence of elongated C_{16}TABr micelles.[4,28,29,37−39] Later, neutron scattering studies[40−42] have shown that the elongation indeed appears already at low concentrations of C_{16}TABr; at 0.10 mol/kg different scattering studies provided $\rho = 1.3$,[40] 1.6,[41] and 2.2[42] for the axial ratio of micelles modeled as prolates. ^{2}H NMR data from this laboratory[11] have largely confirmed the scattering results, yielding $\rho = 1.7$ at 0.12 *m* C_{16}TABr. Moreover, the NMR data have also led to a lateral diffusion coefficient of about 80×10^{-12} m^2/s of the $C_{16}TA^+$ ions. There are three reasons for which we discuss our findings on pure C_{16}TABr micelles below. First, the data narrow the divergence of the neutron scattering results from each other. Second, the results obtained from NMRD[11] are sensitive to the lateral diffusion coefficient D_{lat} of the $C_{16}TA^+$ ions, the value of which can be questioned. Third, it will be stressed once more that NMR relaxation data alone cannot distinguish between prolate and oblate aggregates for small axial ratios.

In the previous work on C_{16}TABr micelles[11] it was possible to exclude oblate shapes for axial ratio $\rho > 2$. This was achieved by fixing the surfactant lateral diffusion coefficient to a constant value (80×10^{-12} m^2/s) for all aggregate shapes and sizes. It should be noted, though, that for a certain micellar solution it is possible to fit both polydisperse distributions of oblates and prolates to the NMRD data if D_{lat} is varied. In neat C_{16}TABr solutions there is a growth in micellar size with increasing concentration. In the polydisperse prolate model this growth can be described with the same D_{lat} as for nearly spherical micelles. In contrast, the polydisperse oblate model requires D_{lat} to increase continuously, up by a factor of 2.5, with increasing concentration.[43] That the surfactant diffusion should be drastically faster for larger aggregates with smaller curvature than for spheres is clearly in conflict with the experimentally determined low values for D_{lat} in cubic phases at high surfactant concentration.[44]

Reflecting the limitations of our model and the limitations of NMR relaxation as a structural tool, fitting our model for the reorientation of the surfactant molecules to experimental NMRDs, presented in Figures 1, 4, and 5, was performed under some assumptions that deserve a longer discussion. To start with, the parameters of relevance to the NMRDs are the various correlation times. For small C_{16}TABr micelles, the correlation times characterizing micellar tumbling and lateral diffusion are rather close to each other, and therefore, they cannot be well separated using the experimental NMRDs. Moreover, τ_{diff} is (from NMRD alone) an inseparable combination of r_{diff} and D_{lat} as described by eq 6. Thus, we must proceed with some plausible assumptions about these involved parameters. The simplest is to set the minor semiaxis r_{hydro} to the all-trans length of the surfactant molecule in neat C_{16}TABr micelles. Hence, τ_m^{rot} values depend solely on the axial ratio ρ,[31] and τ_{diff} is extracted by fitting our model to the experimental data; through eq 6 we can obtain D_{lat}. Without these or other assumptions, the fitted parameters would remain indeterminate.

In a previous ^{2}H NMRD work,[11] the lateral diffusion coefficient of the surfactant was fixed to a particular value, 80×10^{-12} m^2/s, which was extracted from assumedly spherical C_{16}TABr micelles in a 0.06 *m* solution. However, scattering data[40,41] show that the C_{16}TABr micelles even at this low concentration deviate somewhat from spherical shape ($\rho = 1.1$−1.3), and the previously obtained value for the lateral diffusion coefficient might need to be revised. In this paper, we proceed differently with the data analysis. We make use of the existing scattering observations[45] on shape, which indicate prolate and exclude oblate micelles. The scattering data also suggest that the minor axis of the neat C_{16}TABr micelles is close to the length of the $C_{16}TA^+$ ion with a fully extended alkyl chain.[40,41] The existence of small rotund micelles in these solutions is also supported by cryo-TEM.[46] The fact that the phase diagram of C_{16}TABr contains a hexagonal phase[47,48] bordering the isotropic micellar phase is yet another indication of prolate aggregate shapes in the micellar solutions. Therefore, we proceed with prolate micellar models and with the assumption of 2.57 nm for the minor semiaxis r_{hydro}; this value is roughly equal to the length of the all-trans C_{16} chain plus the headgroup diameter. As demonstrated below, NMR relaxation, even though it cannot

TABLE 1: Micellar and Molecular Parameters of C_{16}TABr-α-d_2 in a 0.10 *m* Surfactant Solution, Obtained by Fitting a Prolate Micellar Model[31] to the Experimental NMRD[a]

r_{hydro} (nm)	ρ	$\langle\rho\rangle$	S_{CD}	τ_f (ps)	$D_{lat}/10^{-12}$ (m^2/s)
2.57 (fixed)		1.42 ± 0.04	0.196 ± 0.006	33.1 ± 0.4	90.7 ± 3.5
2.57 (fixed)	1.66 ± 0.04		0.199 ± 0.001	36.5 ± 0.4	120.4 ± 4.7
2.37 (fixed)		1.48 ± 0.04	0.196 ± 0.001	37.0 ± 0.4	66.1 ± 3.2
2.37 (fixed)	1.76 ± 0.04		0.200 ± 0.001	36.3 ± 0.4	96.2 ± 4.3

[a] All fittings have been performed by the Levenberg−Marquardt least-squares algorithm.[58] The minor hydrodynamic semiaxis r_{hydro} of the model has been fixed in all fits to values representing plausible estimates of the all-trans length of the $C_{16}TA^+$ ion. ρ and $\langle\rho\rangle$ are the axial ratios obtained in monodisperse and polydisperse micellar models, respectively. The lateral diffusion coefficient D_{lat} is calculated using eqs 6 and 7. The provided errors are $\pm 2\sigma$ limits, where σ is estimated from the random parameter error as provided by the fit.

always distinguish among shapes, is a sensitive tool to obtain the micellar size once the micellar shape is independently established.

The NMRD for neat C_{16}TABr-α-d_2 micelles in a 0.10 *m* solution is shown in Figure 1. Together with the experimental data, three theoretical fittings with different fixed axial ratio ρ are provided as well. Obviously, the fit quality is sensitive to the selected axial ratio, which is further illustrated in Figure 2. The axial ratio $\rho = 2.2$, obtained by one of the neutron scattering studies,[42] is clearly excluded by our data. Although ^{2}H relaxation is less distinctive toward small ρ, spherical micelles are nevertheless clearly less credible as attested both by the low-frequency R_1 and the high-frequency R_2 data. The axial ratio, favored by our data, is 1.6−1.7, which coincides with one of the recent neutron scattering[41] and the previous NMR findings.[11] (Fixing the minor semiaxis to 2.37 nm provides rather similar results, with the minimum shifted to $\rho \approx 1.7-1.8$.) We note that ^{81}Br NMR relaxation data on the same system[49] suggest a similar axial ratio ($\rho = 1.4-1.6$). Clearly, the experimental data can be well fitted under the assumption of monodisperse micelles. Invoking polydispersity, as by eqs 8 and 9, leads to fits of equally good quality, with an average axial ratio of 1.4 ± 0.1 (Table 1).

The lateral diffusion coefficient can be calculated from the fitted τ_{diff} values via eqs 6 and 7. As shown by Table 1, the obtained D_{lat} depends strongly on the selected value for r_{hydro}. This feature is not surprising, since the rotational correlation times are sensitive functions of the micellar dimensions. To account for a certain NMRD, larger r_{hydro} leads to longer rotational correlation times τ_m^{rot}, which lead to shorter τ_{diff}. The lateral diffusion coefficients, calculated from the fitted τ_{diff}, again depend on the selected r_{hydro}, this time through eqs 6 and 7; a larger radius τ_{diff} yields larger D_{lat}. As a cumulative effect, the obtained lateral diffusion coefficients are approximately power-2.5 functions of the selected micellar dimensions. D_{lat} values, calculated under various assumptions, are presented in Table 1. We consider the value 90×10^{-12} m^2/s obtained for polydiperse prolates with the short axis fixed to 2.57 nm as the best presently available value for C_{16}TABr micelles without solubilizate.

^{2}H Spin Relaxation of C_6D_6 Solubilized in C_{16}TABr Micelles. As indicated primarily by the observed displacements of the various ^{1}H lines of the C_{16}TABr molecule on benzene addition, benzene is preferentially located in or close to the headgroup region of C_{16}TABr micelles.[4,5] Ring-current-induced chemical shift effects of the C_{16}TABr protons depend, however, not only on the concentration of nearby benzene molecules but also on the order parameter that describes their average intermolecular orientation.[10] Thus, the observed strong shift of the ^{1}H lines of methylene and methyl protons in or close to the headgroup and the small shift of the lines of methylene protons far away from the headgroup could also be interpreted as a larger mutual order of the benzene and surfactant molecules in the headgroup region.

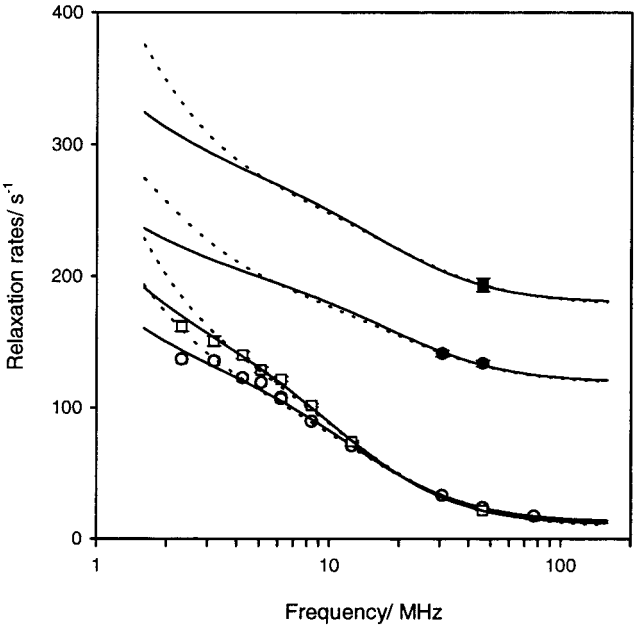

Figure 4. Frequency dependence of the ^{2}H relaxation rates R_1 (empty symbols) and R_2 (full symbols) of C_{16}TABr-α-d_2 in a 0.10 *m* C_{16}TABr solution with $X = 0.8$ (○) and $X = 1.4$ (□) solubilized benzene. Both polydisperse (solid lines) and monodisperse (dotted lines) prolate micellar models were fitted to the data. The fits were performed by fixing the minor semiaxis of the micelles to the length of the all-trans length of the $C_{16}TA^+$ ion (2.57 nm). The fitted parameters are presented in Table 4.

Our ^{2}H spin relaxation results (Figure 3) on dissolved C_6D_6 are not dependent on such effects. The analysis of the data was performed to test the following simple hypothesis: if the solubilized benzene is located predominantly in the headgroup region and therefore diffuses solely along the surface, then its NMRD must provide us with the same axial ratio as the one obtained from the surfactant relaxation. Because of the fast lateral diffusion of benzene, surface diffusion has a dominating influence on the NMRD of C_6D_6. The ^{2}H relaxation rates were measured at the three highest magnetic fields, and the surface diffusion part of the NMRD is well sampled at the corresponding high NMR frequencies.

In contrast to the neat C_{16}TABr case we have no scattering information available about the shape for the benzene-containing micelles. Therefore, benzene-containing samples were also investigated by the cryo-TEM technique. The image in Figure 6 displays small aggregates rather similar to the ones reported for neat C_{16}TABr solutions[46] at about the same concentration and no oblate-like features. In contrast to NMR, cryo-TEM is less model-dependent when qualitatively distinguishing between micellar shapes. Since the micrograph is a 2D projection of a 3D region, oblates can have two major distinct projections:

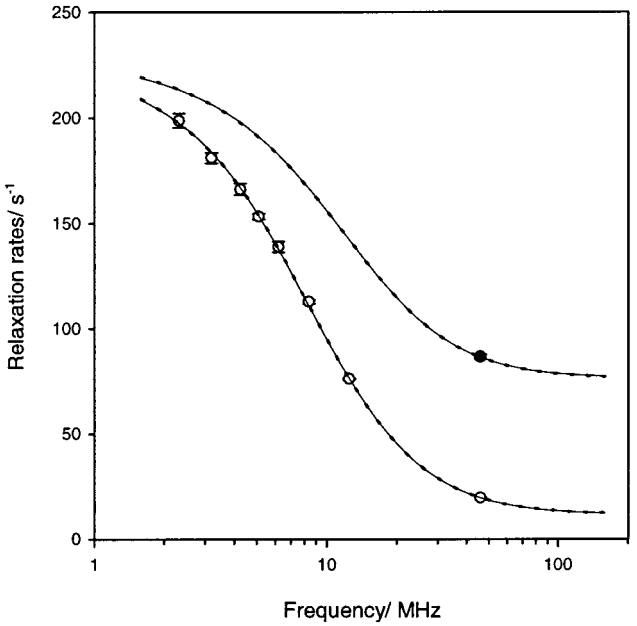

Figure 5. Frequency dependence of the ^{2}H relaxation rates R_1 (○) and R_2 (●) of C_{16}TABr-α-d_2 in a 0.10 *m* C_{16}TABr solution with $X = 2.0$ solubilized benzene. Both polydisperse (solid lines) and monodisperse (dotted lines) prolate micellar models were fitted to the data. The fits were performed by fixing the lateral diffusion coefficient D_{lat} of the $C_{16}TA^+$ ions to the value obtained at $X = 1.4$. The fitted parameters are presented in Table 4.

edge-on and face-on.[50,51] In Figure 6 we do not observe any such different projections, and thus, we conclude that the C_{16}TABr micelles continue to be prolate-shaped also with solubilized benzene.

The results of the fits of a prolate model to the C_6D_6 data with the minor axis fixed to $r_{hydro} = 2.57$ nm (vide supra) and with r_{diff} defined by eq 7 to the benzene relaxation data are given in Figure 3 and Table 2. At low benzene concentration ($X = 0.3$) the obtained axial ratio is 1.4 ± 0.1, which is indeed a value close to the one obtained in pure C_{16}TABr micelles (see Table 1). At higher benzene concentrations ($X = 1.0$), the axial ratios obtained from benzene and C_{16}TABr relaxation (see Table 4) largely coincide. Moreover, the fitted benzene order parameters (about 0.08) are close to the ones obtained from quadrupole-split ^{2}H NMR spectra in hexagonal phases[8] of C_{16}TABr (about 0.09). Hence, our data support the idea of having the benzene molecules mainly located in the headgroup region. The fitted D_{lat} values have large uncertainties, but nevertheless, it is clear that the benzene molecules diffuse significantly faster than the $C_{16}TA^+$ ions.

The obtained fast correlation times τ_f for the local reorientation of the solubilized benzene molecules are about 6−7 ps, much slower than the same correlation times for benzene reorientation[52] in hexadecane (2.9 ps), dodecane (1.8 ps), or benzene (1.4 ps). Obviously, the benzene reorientation is hindered. Our value of τ_f obtained for C_6D_6 molecules in C_{16}TABr micelles is in conflict with previous results.[53] Although they also detected an NMRD for C_6D_6 in C_{16}TABr at $X = 0.1$, the data points of Wasylishen et al.[53] were fewer (only three) and less accurate than ours. Hence, they could analyze their data only within a single-step relaxation model, which has then led to a significant overestimate (17 ps) of τ_f.

Solubilized transdecaline,[54] which was indicated to reside in the micellar interior, seems to be slowed down in its reorientation somewhat less than benzene in C_{16}TABr. The fast motion of deuteriochloroform in alkylammonium micelles[55] was shown to be characterized by $\tau_f = 9-10$ ps, which is considerably higher than the same correlation time for deuteriochloroform in bulk hydrocarbons (~2 ps). Chloroform, however, has a significant dipolar charge distribution that might as well lead to solubilization in the headgroup region.

At $X = 2.0$, the NMRD of C_6D_6 is dramatically different. Qualitative observation of the NMRD in Figure 3 shows that the R_1 and R_2 relaxation rates of benzene converge at around 10 MHz. Therefore, the quadrupole coupling is averaged to zero by processes with correlation times τ_s on the order of 1 ns and there is no residual coupling to be modulated by the slower micellar tumbling as yielded by the ^{2}H relaxation of C_{16}TABr-α-d_2 at $X = 2.0$ (vide infra). Hence, a one-site surface diffusion model (as for C_6D_6 at $X = 0.3$ and 1.0) is clearly not applicable in this case and we find that the relaxation data of C_6D_6 are best described by a simple Lorentzian two-step model with the parameter values given in Table 3. Obviously, the small τ_s value cannot be connected to surface diffusion on an aggregate but rather to translational diffusion of benzene molecules across and within the micelle.

At $X = 2.0$, the distribution of the benzene among various intramicellar regions prevents us from interpreting the observed NMRD within any sophisticated model. The only robust (neither in strong covariance with other model parameters nor much sensitive to the details of the applied model) element of any analysis is the fast correlation time τ_f, which provides the frequency-independent background to NMRD. It is clear from Figure 3 that τ_f must decrease a lot from the value obtained at lower ($X = 0.3$ and 1.0) benzene concentrations. A fit of a simple two-step model to the relaxation data provides $\tau_f = 2.4 \pm 0.9$ ps (Table 3), which indicates near-bulk reorientational dynamics. In fact, this low value of τ_f represents an average of this parameter for benzene molecules exchanging rapidly (on the time scale of the relaxation times) among various intramicellar regions. At the benzene content of $X = 0.3$ and 1.0, where the relaxation data indicated dominating solubilization in the headgroup region, we obtained 6−7 ps for τ_f. In the simplest possible model, we may therefore assume that there are two distinct regions, headgroup and interior. The headgroup region is characterized by $\tau_f = 6-7$ ps, while for the interior region we set τ_f to that of benzene in bulk and in bulk aliphatic hydrocarbons[52] (1−3 ps). In this model, the τ_f data yield 50% as an upper limit for the amount of benzene residing in the headgroup region at a benzene load of $X = 2.0$.

Studying the state of solubilized benzene molecules is, of course, an important part of this work. Nevertheless, the main point with starting the analysis with the relaxation of the solubilized C_6D_6 is that the findings above provide strong support to the models chosen to analyze the surfactant relaxation data in the next section. To recapitulate, at low ($X = 0.3$ and 1.0) benzene content, the benzene dominantly resides at the micellar interface, while at high ($X = 2.0$) benzene content a large part of the solubilized benzene is within the micellar core. Any choice of the micellar radius involved in the analysis below through eqs 5 and 6 must comply with the implications of these findings.

^{2}H Spin Relaxation of C_{16}TABr-α-d_2 in Micelles with Solubilized Benzene. When benzene is solubilized in the C_{16}TABr micelles to mole ratios $X = 0.8$ and $X = 1.4$, the transverse relaxation rate R_2 and the low-frequency longitudinal relaxation rates R_1 of C_{16}TABr-α-d_2 increase (Figure 4), indicating micellar growth. Since benzene at low to moderate mole ratios is dominantly solubilized in the headgroup region of the micelles, it will reduce the headgroup−headgroup

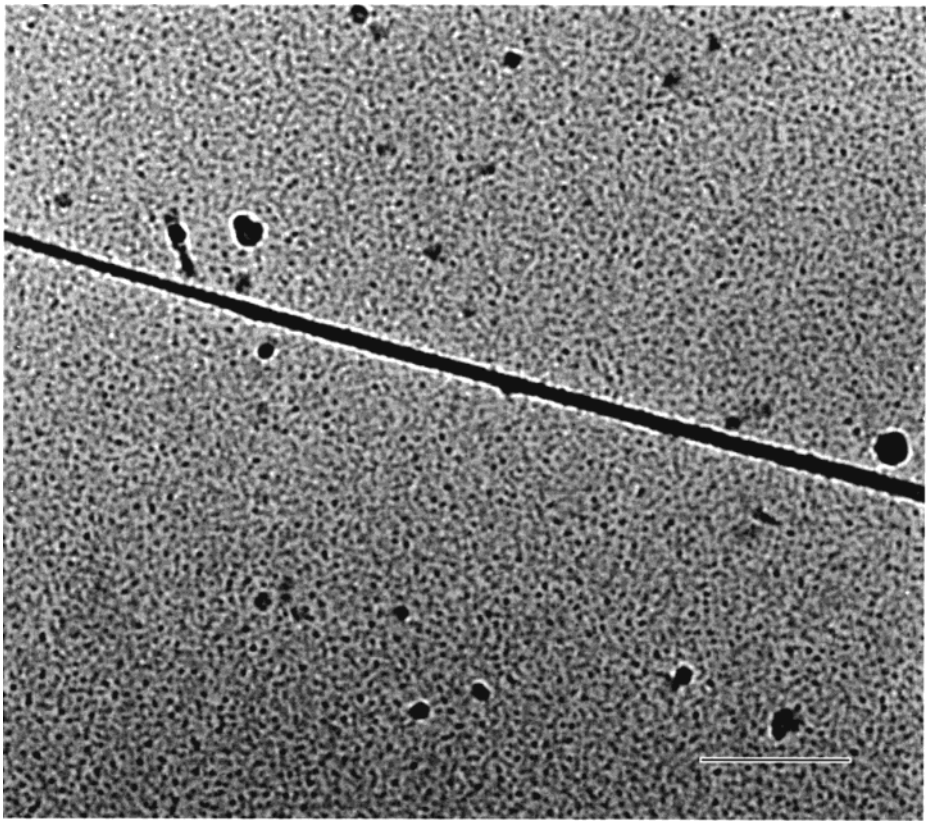

Figure 6. Cryo-TEM micrograph of a frozen solution of 0.10 *m* C_{16}TABr with $X = 1.0$ solubilized benzene. The bar represents 100 nm. (The line running in the middle of the picture is a crack in the sample.)

TABLE 2: Micellar and Molecular Parameters of C_6D_6, Obtained by Fitting a Prolate Micellar Model[31] to the Experimental NMRD[a]

X	r_{hydro} (nm)	$\langle\rho\rangle$	S_{CD}	τ_f (ps)	$D_{lat}/10^{-12}$ (m^2/s)
0.3	2.57 (fixed)	1.30 ± 0.05	0.088 ± 0.014	6.6 ± 1.9	294−815
1.0	2.57 (fixed)	2.69 ± 0.08	0.075 ± 0.004	6.1 ± 0.6	310−561

[a] The minor hydrodynamic semiaxis r_{hydro} of the model has been fixed in all fits to 2.57 nm, which estimates the all-trans length of the $C_{16}TA^+$ ion (see Table 1 and the text for the other parameters). The asymmetric and large uncertainty of the obtained lateral diffusion coefficient is represented by providing the range that contains the values allowed by the experimental random error.

TABLE 3: Results from Fitting of a Lorentzian Two-Step Model to the Experimental NMRD of C_6D_6 in a 0.10 *m* C_{16}TABr Surfactant Solution with Benzene Content $X = 2.0$

S_{CD}	τ_f (ps)	τ_s (ns)
0.086 ± 0.009	2.4 ± 0.9	1.3 ± 0.2

repulsion and thereby possibly also affect the lateral diffusion of the surfactant but to an a priori unknown extent. Moreover, for the C_{16}TABr micelles containing benzene we have, unfortunately, no scattering information available that would allow us to set the minor axis of the micelle to a particular value. It is therefore not possible to apply the same data evaluation strategy as for solubilizate-free micelles.

Because of the strong covariance between D_{lat} and r, we analyze the NMRD data in Figure 4 for the solutions with $X = 0.8$ and $X = 1.4$ under two different sets of limiting hypotheses: (1) Since benzene is mainly located in the headgroup region we may plausibly assume that the minor axis of the micelles is not affected, i.e., we keep it fixed to $r_{hydro} = 2.57$ nm and let D_{lat} vary. (2) We fix D_{lat} to 90×10^{-12} m^2/s, the value for the neat CTAB micelles and let r_{hydro} vary in the fittings. The same model, eq 9, is used for the polydispersity in the axial ratio, and no extra assumptions are made about the eventual polydispersity in the benzene/surfactant ratio among the micelles. The results from the fittings are presented in Table 4. In contrast to the neat C_{16}TABr micelles the polydisperse model has a significantly higher credibility than the monodisperse model (from which therefore results are only shown in Figure 4) for these solutions.

TABLE 4: Micellar and Molecular Parameters of C_{16}TABr-α-d_2 in a 0.10 *m* Surfactant Solution and with Different Amounts of Solubilized Benzene *X*, Obtained by Fitting a Prolate Micellar Model[31] to the Experimental NMRD (See Text for Details)

X	r_{hydro} (nm)	$\langle\rho\rangle$	S_{CD}	τ_f (ps)	$D_{lat}/10^{-12}$ (m^2/s)
0.8	2.57 (fixed)	2.40 ± 0.04	0.209 ± 0.001	32.7 ± 0.5	126 ± 5
	2.29 ± 0.03	2.64 ± 0.05	0.210 ± 0.002	32.6 ± 0.6	90.7 (fixed)
1.4	2.57 (fixed)	2.72 ± 0.05	0.220 ± 0.004	27.6 ± 2.2	110 ± 10
	2.40 ± 0.08	2.89 ± 0.09	0.221 ± 0.005	27.4 ± 2.5	90.7 (fixed)
2.0	3.27 ± 0.06	1.30 ± 0.06	0.209 ± 0.001	29.2 ± 0.8	110 (fixed)

As a result of the fittings according to scheme 1 we find that when r_{hydro} is fixed, we obtain a 30% increase of the lateral diffusion of the surfactant molecules when benzene is present in the micelles. This is a very reasonable result, since the solubilized benzene molecules screen the electrostatic interaction between the headgroups. If D_{lat} is fixed to 90×10^{-12} m^2/s according to scheme 2, we obtain a somewhat smaller r_{hydro} than that for the neat C_{16}TABr micelles, and in this case, there is a slight radial growth upon increasing the benzene content from $X = 0.8$ to $X = 1.4$. In both cases, the micellar growth upon solubilization is mainly axial and the fast (picosecond) dynamics of the α-methylene segment is unchanged on benzene addition as indicated by the roughly constant values of S_{CD} and τ_f.

We must note, though, that because of the covariance between D_{lat} and r_{hydro}, other, perhaps less plausible, combinations of parameter values also provide credible fits; the larger the value the minor semiaxis is fixed to (smaller curvature) the larger becomes D_{lat} (faster surface diffusion). To fit the model with radially swollen micelles, D_{lat} has to be increased dramatically; $r_{hydro} = 3.5$ nm requires $D_{lat} = 250 \times 10^{-12}$ m^2/s, which can be regarded as physically unrealistic in comparison with the values obtained in neat micelles and in liquid crystalline phases of ionic and nonionic surfactants.[32] Although the covariance problem leaves us with a slight ambiguity, one trend is robust: all combinations of r_{hydro} and D_{lat} are consistent with an increase of the average axial ratio upon solubilization with $X = 0.8$ and 1.4. Keeping r_{hydro} below 3.5 nm keeps the average axial ratio greater than 2.2.

At the highest benzene content of this study, $X = 2.0$, a large part of the solubilized benzene is located in the micellar interior. Thus, the minor semiaxis is certainly larger than the value obtained in benzene-free micelles. We can reason, however, that the headgroup layer is saturated with benzene at $X = 1.4$, and therefore, the surfactant lateral diffusion coefficient at even higher benzene concentrations remains close to the value experienced there. Thus, we analyze the NMRD obtained for the $X = 2.0$ system under the assumption of $D_{lat} = 110 \times 10^{-12}$ m^2/s. From the fittings (see Table 4) we obtain almost the same order parameter and fast correlation time as with lower benzene concentrations, which gives some confidence to the evaluation method. The micelles at this high benzene content have grown radially by about 30%, which makes room for the benzene in the micellar core, and decreased in axial ratio to 1.3. These initial microemulsion droplets thus deviate somewhat from spherical shape. From the volumes of the C_{16}TABr and benzene molecules we estimate that the average droplet consists of 250 C_{16}TABr molecules and 500 benzene molecules.

Concluding Remarks

As is well-known, the benzene molecule has a charge distribution with maxima of negative charge density on the two sides of the molecular plane while the rim of the aromatic plane has a positive electrostatic potential. Nearby positive charges interact favorably with the benzene π electrons, creating a rather strong complex. This phenomenon is called cation$-\pi$ "binding".[56] Ab initio calculations[57] have estimated the binding energy between benzene and the tetramethylammonium cation to 9 kcal/mol. Thus, it has been argued that this electrostatic effect is the underlying reason for the observed solubilization behavior of benzene in cationic surfactants, such as C_{16}TABr. The strong interaction of the benzene molecules with the headgroup charges is the probable reason for the slowing down of the picosecond-scale molecular motions of benzene as witnessed by the NMRD of dissolved C_6D_6.

When uncharged molecules, such as benzene, are introduced at the interface, the surface charge density of the micelles decreases, which might lead to a smaller average curvature and, consequently, to elongated micelles. In some other surfactant solutions, mostly with aromatic counterions, such elongation effects are huge; in the present system, however, the NMRDs and the cryo-TEM images exclude the existence of very long, wormlike micelles. Instead, the axial ratio remains below 3. This increasing axial ratio is reflected in the increasing viscosity of the solutions.

Above a certain benzene concentration, however, the surface layer is saturated; in other words, the decreasing electrostatic gain (due to the decreasing coordination of benzene by headgroup cations) cannot compensate for the unfavorable benzene−water contact. Thus, the benzene molecules become increasingly solubilized in the micellar core, which is also manifested by a shorter average correlation time τ_f for the local reorientation of C_6D_6. Parallel to it, the micelles clearly swell beyond the length of a fully extended surfactant molecule.

While this simple picture perhaps suffices to rationalize our observations, the reality is certainly more complex. In particular, the counterions must play an important role; note that the same surfactant but with Cl^- as counterion (i.e., C_{16}TACl) is not showing any dramatic increase of either the viscosity[9] or the R_2 spin relaxation rate[7] on benzene addition. In comparison to chloride, the bromide counterion is closer to the micellar surface and reduces charge of micelles more effectively. Obviously, this may effect the benzene headgroup interaction as well.

Acknowledgment. The Swedish Natural Science Research Council (NFR) has supported this work. N.H. and R.S. thank the Ernst Johnsson Foundation and the Swedish Institute for their respective scholarships. Maria Törnblom is thanked for valuable comments on the manuscript.

References and Notes

(1) *Solubilization in Surfactant Aggregates*; Christian, S. D., Scamehorn, J. F., Eds.; Marcel Dekker: New York, 1995.
(2) Nagarajan, R. *Curr. Opin. Colloid Interface Sci.* **1996**, *1*, 391.
(3) Törnblom, M.; Henriksson, U. *J. Phys. Chem. B* **1997**, *101*, 6028.
(4) Eriksson, J. C.; Gillberg, G. *Acta Chem. Scand.* **1966**, *20*, 2019.
(5) Fendler, J. H.; Patterson, L. K. *J. Phys. Chem.* **1971**, *25*, 3907.
(6) Johansson, L. B. Å.; Lindblom, G.; Nordén, B. *Chem. Phys. Lett.* **1976**, *39*, 128.
(7) Klason, T. NMR-studies of solubilization, hydrocarbon chain motion and the state of water in amphiphile-water systems. Ph.D. Thesis, Royal Institute of Technology, Stockholm, 1983.
(8) Henriksson, U.; Klason, T.; Ödberg, L.; Eriksson, J. C. *Chem. Phys. Lett.* **1977**, *52*, 554.
(9) Larsen, J. W.; Magid, L. J.; Payton, V. *Tetrahedron Lett.* **1973**, *29*, 2663.
(10) Stilbs, P. *J. Colloid Interface Sci.* **1983**, *94*, 463.
(11) Törnblom, M.; Henriksson, U.; Ginley, M. *J. Phys. Chem.* **1994**, *98*, 7041.
(12) Duns, G. J.; Reeves, L. W.; Yang, D. W.; Williams, D. S. *J. Colloid Interface Sci.* **1995**, *173*, 261.
(13) Hirata, H.; Ohira, A.; Iimura, N. *Langmuir* **1996**, *12*, 6044.
(14) Davey, T. W.; Ducker, W. A.; Hayman, A. R.; Simpson, J. *Langmuir* **1998**, *14*, 3210.
(15) Zana, R.; Lévy, H.; Danino, D.; Talmon, Y.; Kwekat, K. *Langmuir* **1997**, *13*, 402.
(16) Bodenhausen, G.; Freeman, R.; Turner, D. L. *J. Magn. Reson.* **1977**, *27*, 511.
(17) Sitnikov, R.; Furó, I.; Henriksson, U. *J. Magn. Reson. A* **1996**, *122*, 76.
(18) Levy, G. C.; Bailey, J. T.; Wright, D. A. *J. Magn. Reson.* **1980**, *37*, 353.
(19) Dubochet, J.; Lepault, J.; Freeman, R.; Berriman, J. A.; Homo, J. C. *J. Microsc.* **1982**, *128*, 219.
(20) Bellare, J. R.; Davis, H. T.; Scriven, L. E.; Talmon, Y. *J. Electron Microsc. Tech.* **1988**, *10*, 87.
(21) Abragam, A. *The Principles of Nuclear Magnetism*; Clarendon: Oxford, 1961.
(22) Davis, J. H.; Jeffrey, K. R. *Chem. Phys. Lipids* **1977**, *20*, 87.
(23) Pyykkö, P. *Ann. Univ. Turku, Ser. A* **1966**, *88*, 93.
(24) Söderman, O.; Walderhaug, H.; Henriksson, U.; Stilbs, P. *J. Phys. Chem.* **1985**, *89*, 3693.
(25) Söderman, O.; Henriksson, U.; Olsson, U. *J. Phys. Chem.* **1987**, *91*, 116.
(26) Ginley, M.; Henriksson, U.; Li, P. *J. Phys. Chem.* **1990**, *94*, 4644.
(27) Furó, I.; Halle, B. *Phys. Rev. E* **1995**, *51*, 466.
(28) Henriksson, U.; Ödberg, L.; Eriksson, J. C.; Westman, L. *J. Phys. Chem.* **1977**, *81*, 76.
(29) Ulmius, J.; Wennerström, H. *J. Magn. Reson.* **1977**, *28*, 309.
(30) Halle, B.; Wennerström, H. *J. Chem. Phys.* **1981**, *75*, 1928.
(31) Halle, B. *J. Chem. Phys.* **1991**, *94*, 3150.
(32) Lindblom, G.; Orädd, G. *Prog. NMR Spectrosc.* **1994**, *26*, 483.
(33) Israelachvili, J. N. *Intermolecular and Surface Forces*, 2nd ed.; Academic Press: San Diego, CA, 1991.

(34) Missel, P. J.; Mazer, N. A.; Benedek, G. B.; Young, C. Y.; Carey, M. C. *J. Phys. Chem.* **1980**, *84*, 1044.
(35) Eriksson, J. C.; Ljunggren, S. *Langmuir* **1990**, *6*, 895.
(36) Nagarajan, R.; Ruckenstein, E. *Langmuir* **1991**, *7*, 2934.
(37) Götz, K. G.; Heckmann, K. *Z. Phys. Chem.* **1959**, *20*, 42.
(38) Reiss-Husson, F.; Luzzati, V. *J. Phys. Chem.* **1964**, *68*, 3504.
(39) Ekwall, P.; Mandell, L.; Solyom, P. *J. Colloid Interface Sci.* **1971**, *35*, 519.
(40) Quirion, F.; Magid, L. J. *J. Phys. Chem.* **1986**, *90*, 5435.
(41) Berr, S.; Jones, R. R. M.; Johnson, J. S. *J. Phys. Chem.* **1992**, *96*, 5611.
(42) Aswal, V. K.; Goyal, P. S. *Physica B* **1998**, *245*, 73.
(43) Törnblom, M. Personal communication.
(44) Eriksson, P. O.; Khan, A.; Lindblom, G. *J. Phys. Chem.* **1982**, *86*, 387.
(45) Hayter, J. B.; Penfold, J. *Colloid Polym. Sci.* **1983**, *261*, 1022.
(46) Lin, Z.; Davis, H. T.; Scriven, L. E. *Langmuir* **1996**, *12*, 5489.
(47) Auvray, X.; Petipas, C.; Anthore, R.; Rico, I.; Lattes, A. *J. Phys. Chem.* **1989**, *93*, 7458.
(48) Wärnheim, T.; Jönsson, A.; Sjöberg, M. *Prog. Colloid Polym. Sci.* **1990**, *82*, 271.
(49) Hedin, N.; Furó, I. *J. Phys. Chem. B* **1999**, *103*, 9640.
(50) Regev, O.; Marques, E. F.; Khan, A. *Langmuir* **1999**, *15*, 642.
(51) Marques, E. F.; Regev, O.; Khan, A.; Miguel, M. G.; Lindman, B. *J. Phys. Chem. B* **1998**, *102*, 6746.
(52) Laaksonen, A.; Stilbs, P.; Wasylishen, R. E. *J. Chem. Phys.* **1998**, *108*, 455.
(53) Wasylishen, R. E.; Kwak, J. C. T.; Gao, Z.; Verpoorte, E.; MacDonald, J. B.; Dickson, R. M. *Can. J. Chem.* **1991**, *69*, 822.
(54) Stilbs, P.; Walderhaug, H.; Lindman, B. *J. Phys. Chem.* **1983**, *87*, 4762.
(55) Canet, D.; Turki, T.; Belmajdoub, A.; Diter, B. *J. Phys. Chem.* **1988**, *92*, 1219.
(56) Gao, J.; Chou, L. W.; Auerbach, A. *Biophys. J.* **1993**, *65*, 43.
(57) Pullman, A.; Berthier, G.; Savinelli, R. *J. Comput. Chem.* **1997**, *18*, 2012.
(58) Press, W. H.; Flannery, B. P.; Teukolsky, S. A.; Vetterling, W. T. *Numerical Recipes*; Cambridge University Press: Cambridge, 1986.